Supporting Information

Dror et al. 10.1073/pnas.1104614108

SI Methods

Methods for Molecular Dynamics Simulations. In all simulations, the receptor was embedded in a hydrated lipid bilayer with all atoms, including those in the lipids and water, represented explicitly. Production simulations were performed on Anton (1), a special-purpose computer designed to accelerate standard molecular dynamics simulations by orders of magnitude. Prior to production simulation, systems were equilibrated using Desmond (2) on a commodity cluster, according to the protocol described below.

System Setup and Simulation Protocol. Simulations of β_2AR were based on the crystal structure of the carazolol-β_2AR complex [Protein Data Bank (PDB) entry 2RH1], and simulations of β_1AR were based on the structure of the cyanopindolol-β_1AR complex (PDB ID entry 2VT4, chain B). The β_2AR crystal structure was determined using a β_2AR-T4 lysozyme (T4L) fusion protein, in which intracellular loop 3 (ICL3) of the receptor was replaced by T4L; the T4L was omitted in our simulations of β_2AR. The crystal structure of β_1AR was determined using a construct with six thermostabilizing point mutations and a deletion of most of ICL3; we back-mutated the six-point mutations to their wild-type residues using Maestro (Schrödinger LLC), but the ICL3 deletion was left unchanged. All chain termini were capped with neutral groups (acetyl and methylamide). The cocrystallized ligands carazolol and cyanopindolol were deleted. Hydrogens were added to the crystal structures using Maestro, as described in previous work (3). All titratable residues were left in the dominant protonation state at pH 7.0, except for Glu122$^{3.41}$ and Asp79$^{2.50}$ in β_2AR and Glu130$^{3.41}$ and Asp87$^{2.50}$ in β_1AR, which were protonated. Asp79$^{2.50}$ and Asp87$^{2.50}$ correspond to rhodopsin Asp83$^{2.50}$, which is protonated during the entire photocycle (4). Glu122$^{3.41}$ and Glu130$^{3.41}$ face the lipid bilayer and thus are likely protonated (3); in addition, a similarly positioned residue in rhodopsin (Glu122$^{3.37}$) is protonated during the entire photocycle (4).

Prepared protein structures were inserted into an equilibrated palmitoyl oleoyl phosphatidyl choline (POPC) bilayer as described in previous work (5), and 10 ligands were placed at arbitrary positions in the aqueous phase, each at least 30 Å away from the binding pocket of the receptor. Chloride ions were added to neutralize the net charge of the system. Simulations of β_2AR under conditions A, C, D, and E (Table S1) initially measured $83 \times 71 \times 87$ Å^3 and contained 131 lipid molecules, 9,706 water molecules, and 14 chloride ions, for a total of approximately 52,000 atoms. Simulations of β_2AR under condition B (Table S1), which had approximately 100 mM NaCl added to the aqueous phase (in addition to the ions present in the previous condition), initially measured $83 \times 83 \times 87$ Å^3 and contained 160 lipid molecules, 11,314 water molecules, 20 sodium ions, and 34 chloride ions, for a total of approximately 60,000 atoms. Simulations of β_1AR (condition F) initially measured $76 \times 77 \times 86$ Å^3 and contained 136 lipid molecules, 9,523 water molecules, 1 sodium ion (from the crystal structure), and 19 chloride ions, for a total of approximately 52,000 atoms. The higher NaCl concentration did not appear to affect the binding pathway.

One system for each of the six conditions was equilibrated using Desmond in the NPT ensemble at 310 K (37 °C) and 1 bar using the Berendsen coupling scheme with 5 kcal mol^{-1} Å^{-2} harmonic-position restraints applied to all non-hydrogen atoms of the protein and ligands; these restraints were tapered off linearly over 5 ns. Unrestrained systems were then simulated for an additional 5 ns to further equilibrate the aspect ratio of the simulation box. During the equilibration process, van der Waals and short-range electrostatic interactions were cut off at 9 Å and long-range electrostatic interactions were computed using the Particle Mesh Ewald method (6) with a $64 \times 64 \times 64$ grid, $\sigma = 2.26$ Å, and fifth-order B-splines for interpolation. All bond lengths to hydrogen atoms were constrained using M-SHAKE (7). A RESPA integrator (8) was used with a time step of 2 fs, and long-range electrostatics were computed every 6 fs.

Production simulations on Anton were initiated from the final snapshot of the corresponding equilibration runs on Desmond, with velocities sampled from the Boltzmann distribution at 310 K, using the same integration scheme, temperature, and pressure. Van der Waals and short-range electrostatic interactions were cut off at 13.5 Å, and long-range electrostatics were computed using the k-space Gaussian Split Ewald method (9) with a $32 \times 32 \times 32$ grid, $\sigma = 3.33$ Å, and $\sigma_s = 2.35$ Å.

Force Field Parameters. The CHARMM27 (10) parameter set with CMAP terms (11) and a recently introduced correction to charged side-chain electrostatics (12) was used for all protein molecules and salt ions in conjunction with the CHARMM TIP3P (13) water model and a modified CHARMM lipid force field (14). Force field parameters for palmitoyl-cysteine were designed previously (3). Force field parameters for dihydroalprenolol, alprenolol, propranolol, and isoproterenol were transferred from aryloxypropanolamine parameter sets previously designed for carazolol (3), and parameters for the alprenolol allyl group were transferred from the model compound 1,4-pentadiene from the CHARMM General Force Field (15). All ligands were simulated in their protonated (ammonium) state. Full parameter sets are available upon request.

Analysis Protocols. Trajectory snapshots, each containing a record of all atom positions at a particular instant in time, were saved every 180 ps during production simulations. Portions of some trajectories were later recomputed to obtain snapshots every 1 ps. Distance and rmsd measurements were computed using the HiMach parallel analysis framework (16).

Ligand rmsd was calculated for the heavy atoms of the ligand after aligning the protein C_α atoms near the binding site (β_2AR residues 109, 110, 113, 114, 117, 118, 193, 203, 207, 286, 289, 290, 293, 312, and 316) to the corresponding atoms in the alprenolol–β_2AR crystal structure. Water traces in Fig. 3 and Fig. 4 were smoothed with a centered 9 ns median filter.

VMD (17) was used to visualize trajectories and to produce Fig. S6; other molecular images were rendered using PyMol (18) and POV-Ray (Persistence of Vision Pty. Ltd.; http://www.povray.org).

Estimating the β_2AR–Alprenolol On-Rate from Simulation. To estimate the k_{on} of β_2AR–alprenolol binding from our simulations, we pooled all 50 simulations under conditions A–C of Table S1 (that is, all simulations involving β_2AR and either alprenolol or dihydroalprenolol, including those where no binding took place; we also calculated such estimates separately for dihydroalprenolol [conditions A–B] and alprenolol [condition C], leading to similar results).

Calculating k_{on} directly is complicated by the fact that the ligand concentration in the aqueous phase of our simulations changes over time; the ligands rapidly partition into the bilayer, and subsequently spend only approximately 2% of their time in the aqueous phase. Because ligands only bind to the receptor via

the aqueous phase, the effective total amount of time during which a ligand has the opportunity to bind to the receptor, T_{eff}, is the total amount of time it spends in the aqueous phase before any ligand has already bound to the receptor. Assuming pseudo-first-order binding kinetics, binding events can be modeled as a Poisson process sampled over an interval of length T_{eff}. Aggregating across the 30 simulations under conditions A and C (which include 9,706 water molecules and 10 ligands) gives $T_{\text{eff,AC}} = 44.1$ μs (total, summed across all ligands). Aggregating across the 20 simulations under condition B (which include 11,314 water molecules and 10 ligands) gives $T_{\text{eff,B}} = 27.6$ μs. A total of 12 binding events were observed in these simulations. The maximum likelihood estimate of the rate of a Poisson process is the number of observed events divided by the time period of observation. For a given number of ligands, the ligand concentration, and thus the rate of the Poisson process under observation, will scale inversely with the number of water molecules in the system. Taking into account the different numbers of water molecules under the different simulation conditions, the maximum likelihood estimate for k_{on} evaluates to 3.1×10^7 $\text{M}^{-1}\,\text{s}^{-1}$ at 37 °C.

Limbird and Lefkowitz (19) measured $k_{\text{off}} \approx 4.3 \times 10^{-3}$ s^{-1} at 37 °C, and presented additional data indicating that $K_D \approx 0.45$ nM under the same conditions. Together, these two values indicate that $k_{\text{on}} \approx 1.0 \times 10^7$ $\text{M}^{-1}\,\text{s}^{-1}$. Contreras et al. (20) measured the association rate directly at a lower temperature (25 °C), obtaining $k_{\text{on}} \approx 3.8 \times 10^6$ $\text{M}^{-1}\,\text{s}^{-1}$.

Calculation of 50% Binding Probability Surface. To compute the "50% binding probability" surface shown in Fig. 3*A*, we performed a trajectory commitment analysis based on all simulations under conditions A–C (Table S1), all of which were initiated with alprenolol far from the receptor surface. All trajectory snapshots were aligned by superimposing the C_α atoms of the transmembrane portions of the seven helices (residues 32–56, 70–94, 106–129, 150–170, 197–220, 275–295, and 307–325), thus establishing a coordinate system relative to the receptor. In this coordinate system, a spatial $16 \times 16 \times 16$ grid of 2-Å voxels was defined over a volume enclosing the extracellular surface of the receptor and the binding pocket. An alprenolol molecule in a simulation was defined as bound to the orthosteric site once its ammonium nitrogen atom sampled a position within 0.5 Å of the position of the alprenolol ammonium nitrogen atom in the aligned crystal structure (PDB entry 3NYA). For each alprenolol molecule in all simulations of β_2AR, an attempt was recorded each time the molecule entered the grid and subsequently exited the grid or went on to bind to the orthosteric site. The voxels visited by the alprenolol ring center on each attempt were identified, and the committor function for binding—the probability that an alprenolol molecule would go on to bind to the orthosteric site before leaving the grid—was estimated for each voxel as the fraction of attempts passing through that voxel that resulted in binding. The resulting spatial committor function maps were smoothed using a 1.5-Å Gaussian blur for visualization purposes (in particular, to compute the 50% binding probability surface).

Calculation of Binding Probabilities Associated with Particular Snapshots. We computed the binding probabilities associated with each of 5 snapshots chosen from simulation 1 (Table S2) by initializing either 10 or 20 additional simulations from each of these snapshots. For each of these additional simulations, all atom positions corresponded to those of the chosen snapshot, but random velocities for each atom were drawn from a Boltzmann distribution. The lengths of these additional trajectories were mostly on the order of 1 μs, although some were as long as 6 μs, giving a total additional simulation time of 113 μs. The binding probability (or committor value) for each snapshot was computed as the fraction of simulations initiated from that snapshot in which the ligand entered the binding pocket before it escaped into bulk solvent. Of the five chosen snapshots, alprenolol was within the extracellular vestibule in four (resulting in binding probabilities of 0.55, 0.70, 0.70, and 0.85) and slightly outside the vestibule in one (resulting in a binding probability of 0.2).

Experimental Data on the Energetic Barrier to Binding. The experimentally determined rate of alprenolol binding to β_2AR ($k_{\text{on}} \approx 1.0 \times 10^7$ $\text{M}^{-1}\,\text{s}^{-1}$ at 37 °C; see "Estimating the β_2AR-alprenolol on-rate from simulation," above) suggests that the process is not diffusion-controlled, as this rate is about two orders of magnitude slower than those typical of diffusion-controlled ligand binding [e.g., $k_{\text{on}} \approx 1.7 \times 10^9$ $\text{M}^{-1}\,\text{s}^{-1}$ for NADH binding to lactate dehydrogenase at 20 °C (21), and $k_{\text{on}} \approx 1 \times 10^9$ $\text{M}^{-1}\,\text{s}^{-1}$ for *N*-methylacridinium binding to acetylcholinesterase at 25 °C (22)].

Further support for this conclusion comes from an estimate of the enthalpic barrier to alprenolol–β_2AR binding based on experimental measurements of the binding free energy (or equivalently, the equilibrium dissociation constant, K_D) and the dissociation kinetics. First, the free energy of alprenolol–β_2AR binding, $\Delta G^\circ = -RT \ln K_D \approx -12.2$ kcal/mol (at 37 °C; 23), sets ΔG° for the bound and unbound ($\Delta G^\circ \equiv 0$) states. In fact, the equilibrium binding free energies of alprenolol and dihydroalprenol to β_1AR and β_2AR are all essentially identical (23–25). These ΔG° values, and the corresponding enthalpy and entropy values determined by van't Hoff analysis for dihydroalprenolol–β_1AR binding ($\Delta H^\circ = -3.5$ kcal/mol, $-T\Delta S^\circ = -8.8$ kcal/mol; 24), are consistent with those determined for structurally diverse beta blockers binding to β_1AR (26). Second, dihydroalprenolol dissociation from β_2AR is reported to exhibit an activation energy of $\Delta E^\ddagger_{\text{dissoc}} = +20.9$ kcal/mol (19); i.e., $\Delta H^\ddagger_{\text{dissoc}} = \Delta E^\ddagger_{\text{dissoc}} - RT = +20.3$ kcal/mol (37 °C). The activation enthalpy of alprenolol association is thus $\Delta H^\ddagger_{\text{assoc}} = \Delta H^\circ + \Delta H^\ddagger_{\text{dissoc}} = +16.8$ kcal/mol. This $\Delta H^\ddagger_{\text{assoc}}$ barrier (of ∼15–20 kcal/mol) is much larger than the apparent enthalpy barriers observed for water self-diffusion ($\Delta E^\ddagger = +4.4$ kcal/mol [$\Delta H^\ddagger \approx +3.8$ kcal/mol]; 27) or the diffusion of (large or small) ligands in water ($\Delta E^\ddagger = +4$ to $+5$ kcal/mol [$\Delta H^\ddagger = +3$ to $+5$ kcal/mol]; 28), indicating that the binding of alprenolol to β_2AR is not diffusion-controlled.

We also performed an Eyring analysis of the same experimental data (19) that suggests (with less confidence, given uncertainty regarding various underlying assumptions) that $\Delta H^\ddagger_{\text{dissoc}} = +18.7$ kcal/mol, and $-T\Delta S^\ddagger_{\text{dissoc}} = +2.7$ kcal/mol. $\Delta G^\ddagger_{\text{dissoc}} = \Delta H^\ddagger_{\text{dissoc}} - T\Delta S^\ddagger_{\text{dissoc}} = +21.4$ kcal/mol, and thus $\Delta G^\ddagger_{\text{assoc}} = \Delta G^\circ + \Delta G^\ddagger_{\text{dissoc}} = +9.2$ kcal/mol. Incorporating ΔH° and $-T\Delta S^\circ$ further suggests that the enthalpy component of the association barrier is $\Delta H^\ddagger_{\text{assoc}} = \Delta H^\circ + \Delta H^\ddagger_{\text{dissoc}} = +15.2$ kcal/mol, in reasonable agreement with the +16.8 kcal/mol derived above. Similarly, the entropy component of the association barrier is $-T\Delta S^\ddagger_{\text{assoc}} = -T\Delta S^\circ - T\Delta S^\ddagger_{\text{dissoc}} = -6.1$ kcal/mol. This entropy gain ($T\Delta S^\ddagger_{\text{assoc}} \approx 5$–10 kcal/mol) linked with the association barrier is suggestive of the release of water from hydrophobic surfaces making a contribution to the association barrier, much as the entropy gain linked with the overall binding process ($T\Delta S^\circ = +8.8$ kcal/mol) is suggestive of the release of water making a contribution to ligand affinity.

Binding Free Energy Calculation. As an additional check of force field accuracy, we computed the dihydroalprenolol–β_2AR binding free energy through simulation using a free-energy perturbation method. The result, -13.4 ± 1.6 kcal/mol, is within error of the value of −12.2 kcal/mol calculated from the experimentally determined K_D of 2.2 nM at 37 °C (throughout, we assume a standard state of 1 M concentration) (29).

The free energy of dihydroalprenolol–β_2AR binding, $\Delta G_{\text{binding}}$, was computed by the double annihilation method (30),

in which $\Delta G_{\text{binding}}$ is computed as the free-energy difference between transfer of the ligand from vacuum into the receptor binding pocket and transfer of the same ligand from vacuum into aqueous solution. The binding pose of the ligand was taken from a snapshot in the simulation of dihydroalprenolol binding to β_2AR, which closely matches the ligand binding pose in the alprenolol–β_2AR complex crystal structure (PDB entry 3NYA); the rmsd of the dihydroalprenolol in that snapshot from its crystallographic position is 0.6 Å. In computing each transfer free energy, Lennard–Jones (LJ) interactions between the ligand and the rest of the system were modeled using a softcore potential (31)

$$V_{\text{softcore}}(r) = 4\epsilon\lambda\left[\left(\frac{1}{\alpha(1-\lambda)^2 + r^6/\sigma^6}\right)^2 - \frac{1}{\alpha(1-\lambda)^2 + r^6/\sigma^6}\right],$$

where $\alpha = 0.5$ and λ is an adjustable parameter; charges on the ligand atoms were scaled by a parameter λ_q. The free-energy difference between the system with $\lambda = 0$, $\lambda_q = 0$ and the system with $\lambda = 1$, $\lambda_q = 1$ are computed for both the ligand in the receptor's binding pocket, ΔG_{pocket}, and the ligand in the aqueous solution, $\Delta G_{\text{solution}}$; the difference between these two values, $\Delta G_{\text{pocket}} - \Delta G_{\text{solution}}$, corresponds to the free energy of binding. As is common in free-energy calculations, a number of intermediate stages with either (*i*) $0 \le \lambda \le 1$ and $\lambda_q = 0$, or (*ii*) $\lambda = 1$ and $0 \le \lambda_q \le 1$, were introduced to achieve better convergence. In simulating the ligand in the receptor at intermediates with $\lambda < 1$, artificial restraints were added to prevent the ligand from wandering away from the binding pocket; the contribution of these restraints to the free energy was corrected using a closed form (30). To achieve better convergence of the free-energy estimate, a few auxiliary intermediates were introduced with $\lambda = 0$, in which the torsional energies, the LJ repulsive energies, and the electric charges of the ligand and the receptor atoms in the ligand's vicinity were scaled down, to better sample the ligand and binding pocket conformations. Intermediates were chosen so as to minimize the statistical errors in the estimated free energies, following a previously outlined procedure (23). All the selected intermediates were simulated in parallel in a replica-exchange simulation, with exchanges between adjacent intermediates attempted every 1 ps. The simulations of the ligand in the receptor were run in Desmond in a constant surface tension ensemble (32) with temperature 310 K, normal pressure of 1 bar, and bilayer surface tension of 0 for about 50 ns per replica; the simulations of the ligand in the aqueous solution were run for 10 ns per replica. The free-energy differences between adjacent intermediates were computed using the Bennett acceptance ratio method (33); statistical uncertainties were estimated by dividing the data into 5 equal time intervals, and computing the standard deviation in the free energies between the intervals.

We also computed free energies for dihydroalprenolol bound to the β_2AR extracellular vestibule. Two different poses of dihydroalprenolol bound in the vestibule—pose 2 and pose 3 in Fig. 2—were selected from binding simulation 1 (Table S2); dihydroalprenolol had remained in each of these poses for over 100 ns during binding. The computed binding free energies were -7.1 ± 1.0 and -7.9 ± 1.2 kcal/mol for poses 2 and 3, respectively. These results indicate that the extracellular vestibule is a favorable ($K_D \approx 5$ μM) metastable binding site for the ligand on its path into the deeper orthosteric site.

1. Shaw DE, et al. (2009) Millisecond-scale molecular dynamics simulations on Anton. *Proceedings of the Conference on High Performance Computing, Networking, Storage and Analysis (SC09)* (ACM, New York).
2. Bowers KJ, et al. (2006) Scalable algorithms for molecular dynamics simulations on commodity clusters. *Proceedings of the ACM/IEEE Conference on Supercomputing (SC06)* (ACM, New York).
3. Dror RO, et al. (2009) Identification of two distinct inactive conformations of the β_2-adrenergic receptor reconciles structural and biochemical observations. *Proc Natl Acad Sci USA* 106:4689–4694.
4. Fahmy K, et al. (1993) Protonation states of membrane-embedded carboxylic acid groups in rhodopsin and metarhodopsin II: A Fourier-transform infrared spectroscopy study of site-directed mutants. *Proc Natl Acad Sci USA* 90:10206–10210.
5. Rosenbaum DM, et al. (2011) Structure and function of an irreversible agonist-β_2 adrenoceptor complex. *Nature* 469:236–240.
6. Darden T, York D, Pedersen L (1993) Particle mesh Ewald: An $N\log(N)$ method for Ewald sums in large systems. *J Chem Phys* 98:10089–10092.
7. Kräutler V, Van Gunsteren WF, Hünenberger PH (2001) A fast SHAKE algorithm to solve distance constraint equations for small molecules in molecular dynamics simulations. *J Comput Chem* 22:501–508.
8. Tuckerman M, Berne BJ, Martyna GJ (1992) Reversible multiple time scale molecular dynamics. *J Chem Phys* 97:1990–2001.
9. Shan Y, Klepeis JL, Eastwood MP, Dror RO, Shaw DE (2005) Gaussian split Ewald: A fast Ewald mesh method for molecular simulation. *J Chem Phys* 122:054101.
10. MacKerell AD Jr, et al. (1998) All-atom empirical potential for molecular modeling and dynamics studies of proteins. *J Phys Chem B* 102:3586–3616.
11. MacKerell AD Jr, Feig M, Brooks CL III (2004) Extending the treatment of backbone energetics in protein force fields: Limitations of gas-phase quantum mechanics in reproducing protein conformational distributions in molecular dynamics simulations. *J Comput Chem* 25:1400–1415.
12. Piana S, Lindorff-Larsen K, Shaw DE (2011) How robust are protein folding simulations with respect to force field parameterization? *Biophys J* 100:L47–L49.
13. Beglov D, Roux B (1994) Finite representation of an infinite bulk system: Solvent boundary potential for computer simulations. *J Chem Phys* 100:9050–9063.
14. Klauda JB, et al. (2010) Update of the CHARMM all-atom additive force field for lipids: Validation on six lipid types. *J Phys Chem B* 114:7830–7843.
15. Vanommeslaeghe K, et al. (2010) CHARMM General Force Field (CGenFF): A force field for drug-like molecules compatible with the CHARMM all-atom additive biological force fields. *J Comput Chem* 31:671–690.
16. Tu T, et al. (2008) A scalable parallel framework for analyzing terascale molecular dynamics simulation trajectories. *Proceedings of the ACM/IEEE Conference on Supercomputing (SC08)* (ACM, New York).
17. Humphrey W, Dalke A, Schulten K (1996) VMD—Visual Molecular Dynamics. *J Mol Graph Model* 14:33–38.
18. DeLano WL (2002) The PyMOL molecular graphics system (DeLano Scientific, San Carlos, CA). http://www.pymol.org.
19. Limbird LE, Lefkowitz RJ (1976) Negative cooperativity among β-adrenergic receptors. *J Biol Chem* 251:5007–5014.
20. Contreras ML, Wolfe BB, Molinoff PB (1986) Kinetic analysis of the interactions of agonists and antagonists with beta adrenergic receptors. *J Pharmacol Exp Ther* 239:136–43.
21. Czerlinski GH, Schreck G (1964) Fluorescence detection of the chemical relaxation of the reaction of lactate dehydrogenase with reduced nicotinamide adenine dinucleotide. *J Biol Chem* 239:913–921.
22. Nolte,H-J, Rosenberry TL, Neumann E (1980) Effective charge on acetylcholinesterase active sites determined from the ionic strength dependence of association rate constants with cationic ligands. *Biochemistry* 19:3705–3711.
23. Shenfeld DK, Xu H, Eastwood MP, Dror RO, Shaw DE (2009) Minimizing thermodynamic length to select intermediate states for free energy calculations and replica-exchange simulations. *Phys Rev E* 80:046705.
24. Severne Y, Kanarek L, Vauquelin G (1986) Agonist-mediated conformational changes of β-adrenoceptors could occur independent of functional coupling to Ns. *Naunyn Schmiedebergs Arch Pharmacol* 332:247–252.
25. Hoffmann C, Leitz MR, Oberdorf-Maass S, Lohse,MJ, Klotz K-N (2004) Comparative pharmacology of human beta-adrenergic receptor subtypes—Characterization of stably transfected receptors in CHO cells. *Naunyn Schmiedebergs Arch Pharmacol* 369:151–159.
26. Weiland GA, Minneman KP, Molinoff PB (1979) Fundamental difference between the molecular interactions of agonists and antagonists with the Beta-adrenergic receptor. *Nature* 281:114–117.
27. Wang JH (1951) Self-diffusion and structure of liquid water. II. Measurement of self-diffusion of liquid water with O^{18} as tracer. *J Am Chem Soc* 73:4181–4183.
28. Longsworth LG (1954) Temperature dependence of diffusion in aqueous solutions. *J Phys Chem* 58:770–773.
29. Caron MG, Lefkowitz RJ (1976) Solubilization and characterization of the β-adrenergic receptor binding sites of frog ethrocytes. *J Biol Chem* 251:2374–2384.
30. Boresch S, Tettinger F, Leitgeb M, Karplus M (2003) Absolute binding free energies: A quantitative approach for their calculation. *J Phys Chem B* 107:9535–9551.
31. Beutler TC, et al. (1994) Avoiding singularities and numerical instabilities in free-energy calculations based on molecular simulations. *Chem Phys Lett* 222:529–539.
32. Feller SE, Pastor RW (1999) Constant surface tension simulations of lipid bilayers: The sensitivity of surface areas and compressibilities. *J Chem Phys* 111:1281–1287.
33. Bennett CH (1976) Efficient estimation of free energy differences from Monte Carlo data. *J Comp Phys* 22:245–268.

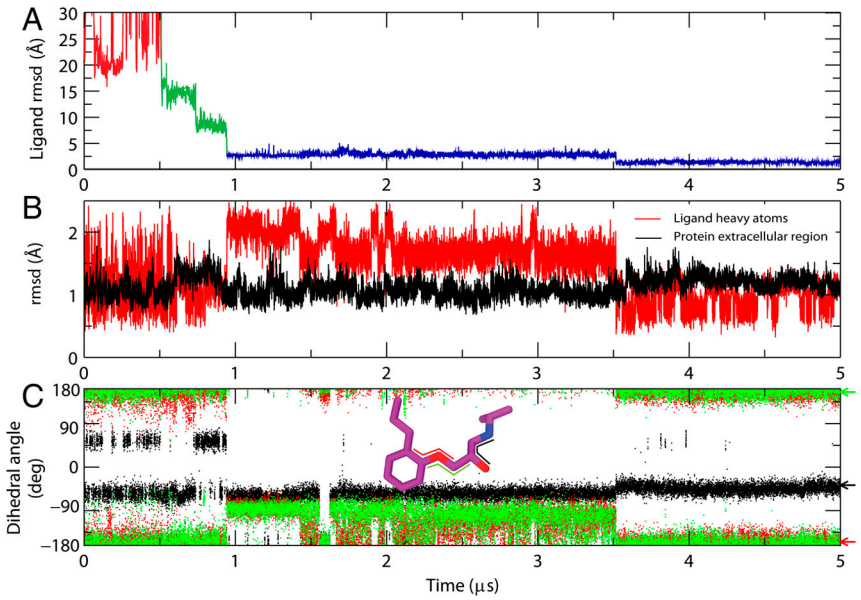

Fig. S1. The entry of alprenolol into the extracellular vestibule does not require any noteworthy structural change in the receptor or the ligand. (*A*) Rmsd of alprenolol in simulation from its position in the alprenolol–β_2AR crystal structure (PDB entry 3NYA), calculated after aligning on protein binding pocket C_α atoms (see *SI Text*). As in Fig. 2*B* of the main text, the colors indicate the location of the ligand relative to the protein: unbound (red), extracellular vestibule (green), and bound in the binding pocket (blue). (*B*) Rmsd of the protein extracellular region (black trace, backbone protein residues 82 to 118, 160 to 210, and 285 to 316) after aligning to the carazalol–β_2AR crystal structure (PDB entry 2RH1), and rmsd of alprenolol's non-hydrogen atoms (red trace) after aligning to corresponding atoms of the bound alprenolol in the 3NYA crystal structure. Incidentally, the reduced variance in ligand rmsd once bound to the protein appears to represent the constraining influence of the protein. The elevated ligand rmsd between approximately 1 and approximately 3.5 μs is due to the ligand being in the binding pocket but twisted near the beta-hydroxyl group (i.e., pose 4 of Fig. 2). (*C*) Three dihedral angles of alprenolol (trace colors correspond to the dihedrals indicated by the thick colored lines in the inset graphic). The data in these plots are from simulation 1 (Table S2).

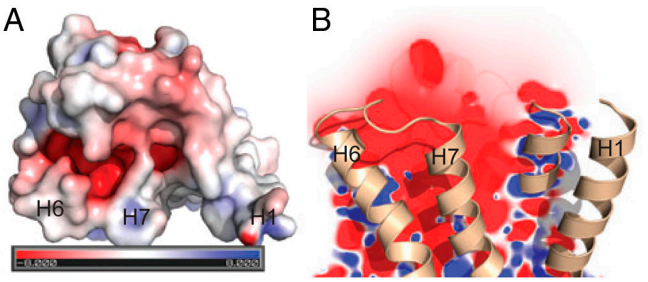

Fig. S2. Electrostatics do not present a barrier to ligand entry into the vestibule. The colors indicate the electrostatic potential (*A*) at the extracellular surface of the protein and (*B*) in a slice through the extracellular half of the receptor. The potential was determined by solving the linearized Poisson–Boltzmann equation at a salt concentration of 150 mM (1). Contours are in units of k_BT/e, where k_B is Boltzmann's constant, T is 310 K, and e is the charge of an electron. All simulated ligands carry a net +1 charge.

1 Baker NA, Sept D, Joseph S, Holst MJ, McCammon JA (2001) Electrostatics of nanosystems: Application to microtubules and the ribosome. *Proc Natl Acad Sci USA* 98:10037–10041.

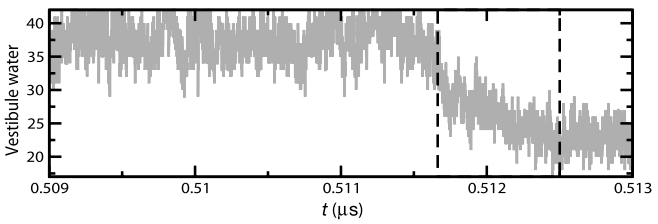

Fig. S3. Water molecules in the extracellular vestibule rapidly evacuate as alprenolol enters. The number of water molecules in the extracellular vestibule is plotted for simulation 1, "zoomed in" to the time when the ligand first enters and associates with this region. The time point when the ligand first enters the vestibule and the time point when it associates with the vestibule's surface are indicated by dashed vertical lines. During ligand entry, approximately 15 water molecules leave the vestibule in less than 1 nanosecond. Here, "vestibule water" (the vertical axis label) refers to the number of water oxygen atoms within an 8 Å radius of the point $(x,y,z) = (-28.7, -2.76, 12.3)$ after the C_α atoms of β_2AR residues 32–56, 70–94, 106–129, 150–170, 197–220, 275–295, and 307–325 were aligned to the crystal structure coordinates (PDB entry 2RH1).

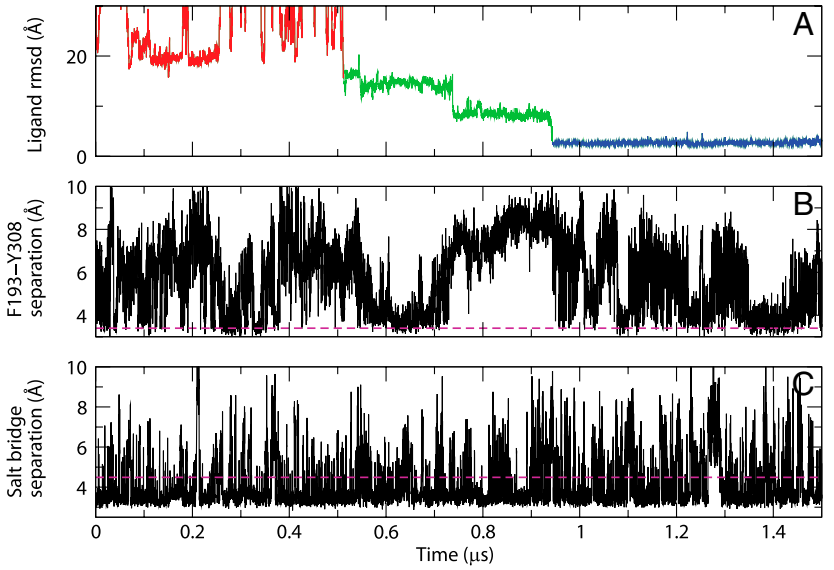

Fig. S4. Receptor conformational changes do not limit the rate of alprenolol movement from the vestibule into the binding pocket. Structural changes from the receptor's crystallographic conformation (in particular, separation of Phe193^{ECL2} from Tyr308$^{7.35}$, and breaking of the Asp192^{ECL2}–Lys305$^{7.32}$ salt bridge) occur before alprenolol moves from the vestibule into the binding pocket, but these changes do not appear to be rate-limiting. The ligand's rmsd from its final bound pose (*A*) is juxtaposed with (*B*) the minimum distance between the non-hydrogen atoms of the side chains of Phe193^{ECL2} and Tyr308$^{7.35}$ and (*C*) the distance between Asp192^{ECL2} C_γ and Lys305$^{7.32}$ N_ζ. While the ligand waits in the extracellular vestibule (approximately 0.52 to approximately 0.94 μs), the side chains of Phe193^{ECL2} and Tyr308$^{7.35}$ remain separated for approximately 200 ns (approximately 0.75–0.94 μs) and the salt bridge breaks and reforms over 200 times. The breaking and forming rates of he salt bridge are 10^8 and 10^9 s^{-1}, respectively (calculated with a salt bridge cutoff of 4.5 Å), while the rate of ligand entry into the binding pocket from the extracellular vestibule (estimated from residence times of ligands in the vestibule in multiple trajectories) is 10^6 s^{-1}. The dashed magenta lines in (*B*) and (*C*) indicate the values of these observables in the alprenolol–β_2AR complex crystal structure (PDB entry 3NYA). Data are from simulation 1.

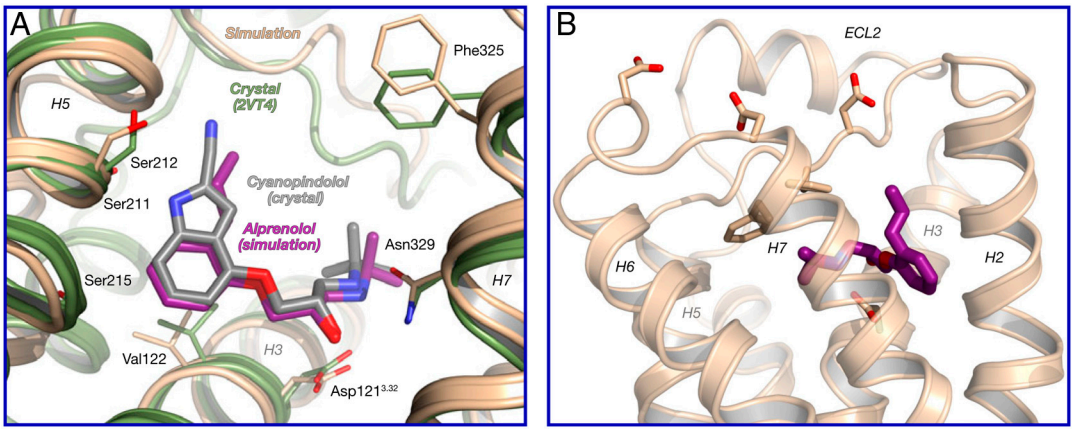

Fig. S5. Alprenolol binds spontaneously to β_1AR in unbiased molecular dynamics simulations, adopting the crystallographically observed pose in some simulations and an alternative pose in others. (*A*) Dihydroalprenolol-bound β_1AR pose from simulation 18 (tan) superimposed on the cyanopindolol-β_1AR complex crystal structure (PDB entry 2VT4; gray). (*B*) Dihydroalprenolol-bound β_1AR pose from simulation 21; this pose is similar to that of Fig. 2, pose 4′.

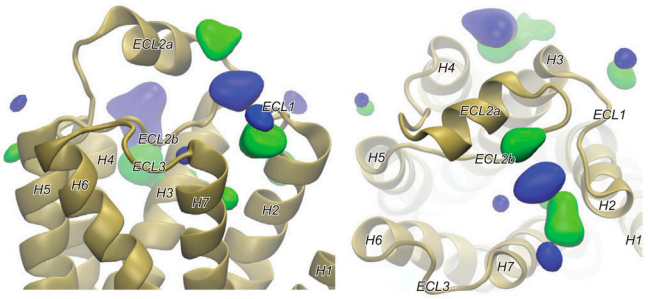

Fig. S6. Alprenolol aromatic ring and ammonium group occupancies in simulations without a binding event show other potential allosteric binding sites. Twenty percent isosurface of alprenolol ammonium group (blue) and ring center (green) over all simulations under conditions *A*–*C* (Table S1) in which an alprenolol molecule did not bind to the orthosteric site. Density maps were computed using the VolMap tool in VMD (17).

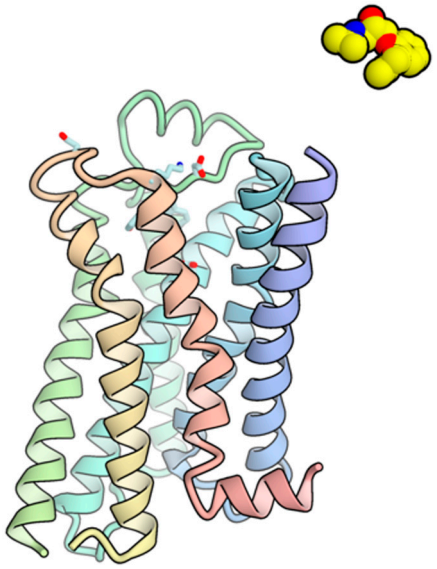

Movie S1 A movie of alprenolol binding to β_2AR, based on simulation 1. For clarity, the lipid bilayer, ions, and water molecules are not shown. The movie plays at 4.5 ns per frame until 0.98 μs, after which it plays at 22.5 ns per frame (i.e., five times faster). The Cartesian components of the protein C_α positions were smoothed using a Gaussian filter ($\sigma = 18$ ns). For the ligand, no smoothing was applied for the first 110 frames of the animation (time = 0.0–0.98 μs). For the remainder of the animation, both the Cartesian components of the ligand atom positions and the internal angles were smoothed using Gaussian filters, with σ values of 8.1 ns and 18 ns, respectively. The movie was created using OpenStructure (1).
Movie S1 (AVI)

1 Biasini M, et al. (2010) OpenStructure: A flexible software framework for computational structural biology. *Bioinformatics* 26:2626–2628.

Table S1. Simulation conditions and durations

Condition	Ligand	Na^+	Cl^-	Num.	Durations (μs)
β_2AR					
A	dihydroalprenolol	0	14	20	5.0, 10.9, 18.9, 1.0, 2.0, 1.0, 1.0, 1.0, 3.0, 3.0, 3.0, *1.0*, *1.0*, *1.0*, *1.0*, *1.0*, *5.0*, *9.0*, *1.0*, *1.5*
B	dihydroalprenolol	20	34	20	6.0, 3.0, 3.0, 1.0, 1.5, 1.0, 1.0, 1.0, 1.0, 2.0, 1.0, 1.0, 1.0, 1.0, 1.0, 5.0, 3.0, 5.0, 1.0, 1.0
C	alprenolol	0	14	10	1.0, 1.0, 1.0, 1.0, 1.0, 3.0, 1.0, 1.0, 1.0, 3.0
D	propranolol	0	14	21	1.0, 1.0, 1.0, 1.0, 1.0, 1.0, 5.0, 1.0, 1.0, 1.0, 1.0, 5.0, 1.0, 1.0, 1.0, 2.1, 1.0, 1.0, 2.6, 1.0, 5.0
E	isoproterenol	0	14	1	15.0
β_1AR					
F	dihydroalprenolol	1	19	10	10.7, 6.0, 6.0, 6.0, 1.0, 2.8, 6.0, 6.0, 1.0, 10.0

All simulations listed in this table were initiated with 10 ligands placed at arbitrary positions in the aqueous phase, each at least 30 Å away from the binding pocket. The third and fourth columns indicate the number of Na^+ and Cl^- ions in each simulation cell, whereas the fifth indicates the number of independent simulations performed under each condition. The durations shown in italics in condition A denote simulations in which weak (0.5 kcal mol^{-1} Å^{-2}) harmonic restraints were applied to the C_α atoms of residues 54–59, 68–73, 131–136, 148–153, 224–229, 267–272, and 323–328 to keep the protein centered and oriented in the simulation box; these restraints were imposed to facilitate certain analyses and did have any noticeable effect on the binding pathway. The single sodium ion in condition F is from the crystal structure of β_1AR.

Table S2. Simulations with binding events

Simulation	Ligand	Condition	Duration (μs)	Final pose	Other poses
β_2AR					
1	dihydroalprenolol	A	5.0	5	—
2	dihydroalprenolol	A	3.0	5	—
3	dihydroalprenolol	A	10.9	4′′	4′
4	dihydroalprenolol	A	4.0	5	—
5	dihydroalprenolol	A	10.0	4′	—
6	dihydroalprenolol	A	5.0	5	4′
7	dihydroalprenolol	A	9.0	4′	—
8	dihydroalprenolol	B	5.0	4′′	—
9	dihydroalprenolol	B	3.0	5	—
10	dihydroalprenolol	B	5.0	4′′	—
11	alprenolol	C	3.0	5	4′′
12	alprenolol	C	3.0	4′′	—
13	propranolol	D	5.0	4′′	—
14	propranolol	D	5.0	4′′	—
15	propranolol	D	5.0	5	4′, 4′′
16	isoproterenol	E	15.0	4	—
β_1AR					
17	dihydroalprenolol	F	10.7	4′	—
18	dihydroalprenolol	F	6.0	5	—
19	dihydroalprenolol	F	6.0	4′	—
20	dihydroalprenolol	F	6.0	4′	—
21	dihydroalprenolol	F	10.0	5	4′, 4′′

Letters in the "Condition" column refer to simulation conditions listed in Table S1. The "Final pose" column indicates the pose at the end of the simulation, whereas the "Other poses" column indicates other poses the ligand adopted while in the binding pocket. The symbols in these two columns refer to poses shown in Fig. 2.

Table S3. A majority of the solvent-accessible surface area lost by the protein and the ligand during the binding process is lost upon ligand entry into the extracellular vestibule.

	Average ligand SASA loss (Å^2)	Average protein SASA loss (Å^2)
Extracellular vestibule	338	165
Binding pocket	415	185

Entries in the table indicate the solvent-accessible surface area (SASA) loss relative to the state when all ligands are in bulk solvent. These SASA values (1) are computed from simulation 1 using the program AREAIMOL from the CCP4 program suite (2) and correspond to the hydrophobic surface area (i.e., carbon SASA) lost by the protein and the ligand.

1 Lee B, Richards FM (1971) The interpretation of protein structures: Estimation of static accessibility. *J Mol Biol* 55:379–400.
2 Collaborative Computational Project, Number 4 (1994) The CCP4 suite: Programs for protein crystallography. *Acta Cryst D Biol Crystallogr* 50:760–763.